

# Fully Transformer Networks for Semantic Image Segmentation

Sitong Wu<sup>1,2\*</sup>, Tianyi Wu<sup>1,2\*</sup>, Fangjian Lin<sup>1,2,3\*</sup>, Shengwei Tian<sup>3</sup>, Guodong Guo<sup>1,2†</sup>

**Abstract**—Transformers have shown impressive performance in various natural language processing and computer vision tasks, due to the capability of modeling long-range dependencies. Recent progress has demonstrated that combining such Transformers with CNN-based semantic image segmentation models is very promising. However, it is not well studied yet on how well a pure Transformer based approach can achieve for image segmentation. In this work, we explore a novel framework for semantic image segmentation, which is encoder-decoder based Fully Transformer Networks (FTN). Specifically, we first propose a Pyramid Group Transformer (PGT) as the encoder for progressively learning hierarchical features, meanwhile reducing the computation complexity of the standard Visual Transformer (ViT). Then, we propose a Feature Pyramid Transformer (FPT) to fuse semantic-level and spatial-level information from multiple levels of the PGT encoder for semantic image segmentation. Surprisingly, this simple baseline can achieve better results on multiple challenging semantic segmentation and face parsing benchmarks, including PASCAL Context, ADE20K, COCO-Stuff, and CelebAMask-HQ. The source code will be released on <https://github.com/BR-IDL/PaddleViT>.

**Index Terms**—Semantic Segmentation, Pyramid Group Transformer, Feature Pyramid Transformer.

## I. INTRODUCTION

SEMANTIC image segmentation aims to assign a semantic label to each pixel in an image, which is an indispensable component for many applications, such as autonomous vehicles [13], human-computer interaction [22], and medical diagnosis [20]. Since the era of deep learning, convolutional neural networks (CNNs) have been the cornerstone of tremendous image segmentation models.

Inspired by successful applications of Transformer [53] on natural language processing tasks (machine translation [42], text classification [25]), and computer vision tasks (image classification [16], [33], [37], [52], [55], [58], [74]), Transformer has attracted more and more interests in the context of semantic image segmentation [37], [46], [55], [64], [77] recently. These methods combined the Transformer block into the encoder-decoder architecture, where the encoder reduces the feature maps and captures rich semantic representations, while the decoder gradually recovers the spatial information

or fuses multi-scale features for generating accurate pixel-level predictions. These approaches can be divided into three categories: (1) **Transformer-CNN architecture** [37], [46], [55], [77]. It contains a Transformer encoder and CNN decoder. Images are first divided into a set of patches and projected to patch embeddings, which are then passed through a Transformer encoder and a traditional CNN decoder to recover the pixel-level prediction, as shown in Figure 1(a). (2) **Hybrid-CNN architecture** [77]. As shown in Figure 1(b), its decoder is the traditional CNN, while the encoder is a combination of CNN (e.g., ResNet [24]) and Transformer layers, in which the output of CNN with a lower resolution is directly used as the patch embeddings for Transformer layers. (3) **Hybrid-Transformer architecture** [64]. It further replaced the CNN decoder of Hybrid-CNN architecture with a Transformer decoder, as shown in Figure 1(c).

Different from the architectures mentioned above, we propose Fully Transformer Networks (FTN) for semantic image segmentation, without relying on CNN. As shown in Figure 1(d), both the encoder and decoder in the proposed FTN are composed of multiple Transformer layers. Firstly, we propose a new Vision Transformer encoder called Pyramid Group Transformer (PGT). Inspired by the hierarchical nature of the features in deep networks [70]), we propose to gradually increase the receptive fields rather than keep it global throughout the whole network (such as ViT [16]). Specifically, PGT spatially divides the feature maps into multiple groups, and performs multi-head self-attention within each group. The receptive fields can be easily controlled by the group number, thus we progressively increase the number of groups, forming a pyramid pattern, to achieve gradually increasing receptive fields. Benefited by such design, our PGT is good at learning hierarchical features, including low-level (edge/color conjunctions), mid-level (complex invariances, similar textures), and high-level (entire objects). Furthermore, PGT can also reduce the unaffordable computational and memory costs of the standard Visual Transformer (ViT), which is essential for pixel-level prediction tasks. Secondly, we propose a Transformer-based decoder, named Feature Pyramid Transformer (FPT) to fuse semantic-level and spatial-level information from multiple levels of the PGT encoder. Benefited by the long-range modeling capacity of Transformer architecture, FPT can capture richer context information. Based on the proposed encoder and decoder, we develop Fully Transformer Networks (FTN) for semantic image segmentation, and evaluated the effectiveness of our approach by conducting extensive ablation studies. Furthermore, we evaluate our FTN on three challenging semantic segmentation benchmarks, including PASCAL-Context [43],

Manuscript created November, 2021. \* denotes equal contribution. (Corresponding author: Guodong Guo).

Sitong Wu, Tianyi Wu, Fangjian Lin, and Guodong Guo are with Institute of Deep Learning, Baidu Research, Beijing 100085, China, and also with National Engineering Laboratory for Deep Learning Technology and Application, Beijing 100085, China (email: wusitong@baidu.com; wutianyi01@baidu.com; linfangjian@baidu.com; guogudong01@baidu.com). Fangjian Lin and Shengwei Tian are with School of Software, XinJiang University, urumqi, China. (email: tianshengwei@163.com).

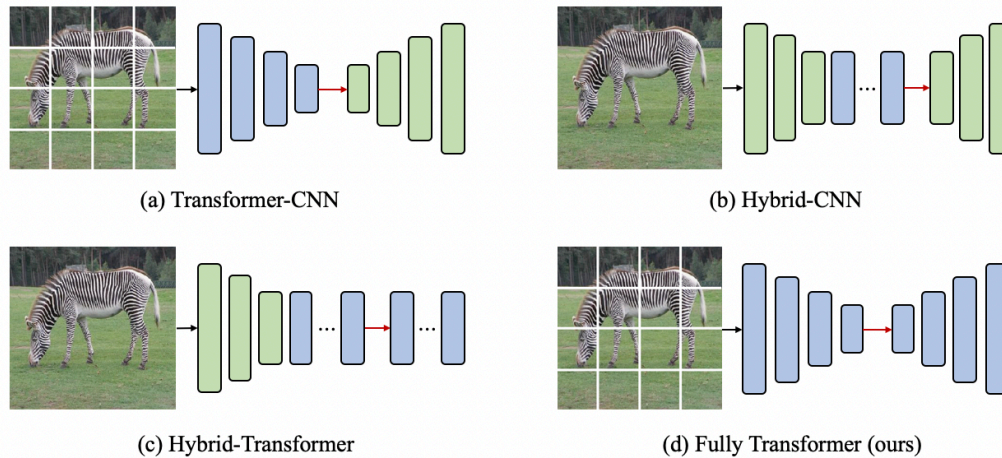


Fig. 1. Pipelines of the previous Transformer-based segmentation models. The blue bar represents Transformer blocks and the green bar indicates CNN layers. The encoder and decoder are separated by a red snip.

ADE20K [78], and COCO-Stuff [5], achieving the state-of-the-art performance (mIoU) of 56.05%, 51.36%, and 45.89%, respectively.

Our main contributions include:

- We propose the Pyramid Group Transformer (PGT) to learn hierarchical representations by gradually increasing the receptive fields via a pyramid pattern. Meanwhile, it can reduce the computation and memory costs of the standard ViT significantly.
- We develop a Feature Pyramid Transformer (FPT) decoder to fuse semantic-level and spatial-level information from multiple levels of the PGT encoder. It is able to capture richer contextual information benefited by the long-range dependencies modeling capability of Transformer architecture.
- Based on the proposed PGT and FPT, we create Fully Transformer Networks (FTN) for semantic image segmentation, which achieves superior performance than previous approaches on multiple challenging benchmarks, including PASCAL Context, ADE20K, COCO-Stuff, and CelebAMask-HQ.

## II. RELATED WORKS

**Semantic Image Segmentation.** The early FCN [38] used a fully convolutional network to generate dense predictions for images with an arbitrary size, which is regarded as a milestone in semantic segmentation. Since then, lots of works have been designing segmentation networks based on CNN architecture [2], [7], [15], [19], [23], [27], [30], [54], [60], [61], [75], [76]. For more precise segmentation, some works [2], [44] were devoted to involving fine-grained details via various hierarchies of decoders. Considering that the effective receptive fields of CNN architecture are proved to be much smaller than its theoretical value [41], some works focused on how to capture more contextual information for a better scene understanding [7]–[9], [61], [76]. For example, DeepLab family [7]–[9] replaced partial pooling layers with atrous convolution to expand the receptive field without reducing the

resolution. PSPNet [76] proposed a general pyramid pooling module to fuse features under four different pyramid scales. CGNet [61] learns the joint features of both local features and the surrounding context in all stages of the network. Recently, in order to aggregate more precise contextual information, [68] and [73] devote to capture class-dependent context information. [29], [36], and [66] proposed to augment each pixel representation by aggregating intra-class and inter-class context respectively. Besides, there are also some works committed to improving the segmentation on the boundary region [4], [11], [69].

**Self-attention in Semantic Image Segmentation.** Inspired by the success of Transformer [53] for NLP tasks, DANet [18] employed the self-attention [56] on the CNN-based backbone, which adaptively integrated local features with their global dependencies. The traditional self-attention serves as a particularly useful technique for semantic segmentation while being criticized for its prohibitive computation burdens and memory usages. To address this issue, [28] and [79] introduced a criss-cross attention mechanism and pyramid sampling module into the self-attention, respectively, aiming to reduce the computation cost and memory usage while keeping the performance. AANet [3] proposed an attention-augmented convolution architecture by concatenating convolutional feature maps with a set of feature maps produced via self-attention. In contrast to these methods which augmented a CNN-based encoder with a self-attention module for semantic segmentation, we propose the novel Fully Transformer Networks, where both encoder and decoder are based on pure Transformer with our specialized design.

**Transformer in Vision Tasks.** DETR [6] combined a common CNN with Transformer for predicting objects, which formulates object detection as a dictionary lookup problem with learnable queries. Later, many researchers explored to adopt a pure Transformer architecture for computer vision tasks [16], [17], [33], [37], [52], [55], [58], [74]. Vision Transformer (ViT) [16] is the first work to introduce a pure Transformer into image classification by treating an image as a sequence of

patches. Recently, Transformer has attracted more and more attention in semantic segmentation [46], [64], [77]. SETR [77] attempted to introduce Transformer for semantic segmentation by using ViT as the encoder and employing CNN-based decoders for generating segmentation results. Trans2Seg [64] stacked a convolution-free encoder-decoder network on top of a common CNN encoder for transparent object segmentation. DPT [46] assembled tokens from multiple stages of ViT and progressively combined them into full-resolution predictions using a convolutional decoder. Different from these approaches that used Transformer as an encoder or decoder, we proposed the encoder-decoder based Fully Transformer Networks for semantic segmentation.

### III. METHOD

In this section, we first describe our framework, Fully Transformer Networks (FTN). Then, we present the encoder architecture of FTN, *i.e.*, Pyramid Group Transformer (PGT), which aims to extract hierarchical representations. Finally, we present the decoder architecture of FTN, *i.e.*, Feature Pyramid Transformer (FPT), which fuses the multi-scale features from the encoder and generates the fine pixel-level predictions.

#### A. Framework of FTN

The overall framework of our FTN is shown in Figure 2, which consists of Pyramid Group Transformer (PGT) encoder and Feature Pyramid Transformer (FPT) decoder. PGT aims to extract hierarchical representations. It is configured with four stages for learning hierarchical features, similar to some classic backbones [24], [65]. Each stage of PGT has a similar structure, which contains a patch transform layer and multiple PGT blocks. The patch transform layer is employed to reduce the number of tokens. In particular, given an input image  $x \in \mathbb{R}^{H \times W \times 3}$ , it is first transformed into  $\frac{HW}{4^2}$  patches with dimension  $C$  by the patch transform layer in stage 1, then the output is fed into  $N_1$  PGT blocks, where  $N_1$  indicates the number of PGT blocks in stage 1. The output of the last block in stage 1 is  $F_1 \in \mathbb{R}^{\frac{HW}{4^2} \times C}$ . For the last 3 stages, the patch transform layer merges each  $2 \times 2$  non-overlapping neighboring patches to reduce the resolution by 1/2 and expand the dimension twice. The output feature in stage  $i$  is  $F_i \in \mathbb{R}^{\frac{HW}{2^{2i+2}} \times 2^{i-1}C}$ . After getting multi-scale features, we employ FPT decoder to fuse semantic-level and spatial-level information from multiple levels. Finally, the output of FPT is fed into a linear layer followed by a simple bilinear upsampling to generate the probability map for each pixel. The pixel-level segmentation result is obtained by argmax operation on the probability map.

#### B. Pyramid Group Transformer

As shown in Figure 2, PGT has four hierarchical stages that generate features with multiple scales. At the beginning of each stage, the features are first shrunk spatially and enlarged in channel dimension by the patch transform layer, and then be fed into the subsequent PGT blocks to learn discriminative representations. PGT progressively increases

the receptive field of self-attention when the stage increases, so as to learn low-level spatial details at shallow layers and high-level semantic features at deep layers. Such a mechanism is superior to the previous Vision Transformer (ViT) [16] where the self-attention with a global receptive field is performed on the whole input features at all layers. Besides, our approach can reduce the computational and memory cost of the whole transformer block, which is desired especially for dense prediction tasks.

Specifically, each feature map is firstly divided into non-overlapping grids and each grid is regarded as a group. Then, self-attention is performed among patches within each group. Thus, patches in one group are unacceptable for patches in other groups, which is equivalent to local receptive fields. Explicitly, the size of each receptive field can be conveniently controlled by the group numbers. As shown in Figure 3, different from the global receptive fields in all stages of ViT [16] and PVT [55], the receptive fields at different stages of our PGT present a pyramid pattern, and we set a consistent receptive field inside each stage. It is notable that the global receptive field is better to be applied in both stage 3 and stage 4 for the reason that features with stride 16 and 32, usually contain rich semantics. For the  $l$ -th PGT block, its computation can be formulated as follows:

$$\begin{aligned}\hat{Z}^l &= Z^{l-1} + \text{PG-MSA}(\text{LN}(Z^{l-1})), \\ Z^l &= \hat{Z}^l + \text{MLP}(\text{LN}(\hat{Z}^l)),\end{aligned}\quad (1)$$

where  $Z^{l-1}$  is the output of the  $(l-1)$ -th PGT block. LN and MLP refer to layer normalization [1] and multi-layer perceptron, respectively. Furthermore, the core of PGT blocks is the Pyramid Group Multi-Self Attention (PG-MSA), which can be formulated as follow:

$$\begin{aligned}\text{PG-MSA}(Z) &= \text{Concat}(h_0, h_1, h_{H-1}), \\ h_i &= \text{Reshape}(\text{head}_i^0, \text{head}_i^1, \dots, \text{head}_i^{G-1}), \\ \text{head}_i^j &= \text{Attention}(Q_i[j], K_i[j], V_i[j]),\end{aligned}\quad (2)$$

where  $i \in \{0, 1, \dots, H-1\}$  is the head index;  $j \in \{0, 1, \dots, G-1\}$  is the group index;  $\text{Attention}(\cdot)$  is the self-attention operation [53].  $Q_i = ZW_i^q$ ,  $K_i = ZW_i^k$ , and  $V_i = ZW_i^v$  indicate the query, key, value embedding of the  $i$ -th head, respectively.

**PGT Variants.** We designed 4 variants with different sizes, named PGT-T, PGT-S, PGT-B, and PGT-L respectively. For a fair comparison, the sizes of these variants are similar to the previous works [37], [52], [55]. The detailed configuration of our PGT variants are shown in Table I, where the definitions of hyper-parameters are listed below:

- $P_i^2$ : the token number reduction factor of the patch transform layer in stage  $i$ ;
- $C_i$ : the dimension of tokens in stage  $i$ ;
- $N_i$ : the number of PGT blocks in stage  $i$ ;
- $G_i$ : the group number of PG-MSA in stage  $i$ ;
- $H_i$ : the head number of PG-MSA in stage  $i$ ;
- $E_i$ : the dimension expansion ratio of MLP in stage  $i$ ;

According to the differences among these variants, the representation capacity is only enlarged by increasing the depth of PGT blocks and the dimension of patch tokens

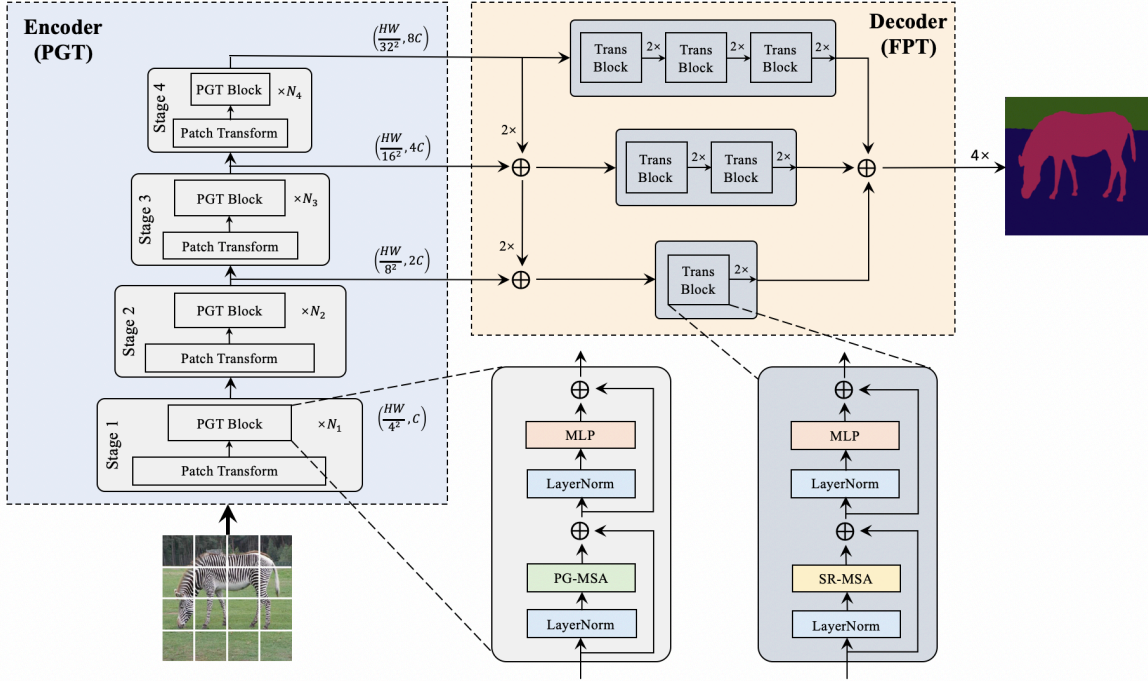


Fig. 2. The overall architecture of our Fully Transformer Networks (FTN). Both the encoder and decoder of FTN are based on Transformer architectures.

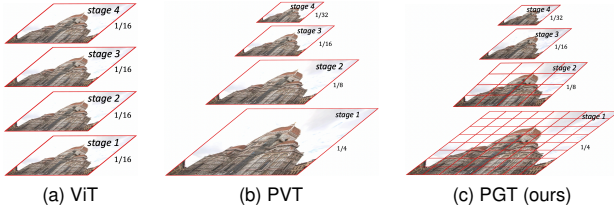


Fig. 3. Comparisons of different self-attention mechanisms in Transformers. (a) ViT performed the global self-attention within the single-scale feature maps throughout the whole network. (b) PVT introduced the pyramid structure to generate multi-scale feature maps and applied the global self-attention to features as well. (c) In PGT, the feature map is first divided into groups in the spatial domain and then the global self-attention is only performed within each group, i.e., a red grid in the figure. The receptive fields (group size) of attention are progressively increased in stages as a pyramid pattern.

(i.e. deeper and wider). For example, PGT-S is obtained by increasing the dimensions of PGT-T, and PGT-B is a deeper version of PGT-S. PGT-L is the deepest and widest among these all. For all variants, the expansion ratio of MLP is set to 4, and the dimension of each head is 32. The pyramid structure of the receptive fields in attention is also consistent for different variants, with group numbers 64, 16, 1, and 1, respectively, in four stages.

**Compared with Swin Transformer.** For Swin Transformer [37], the window size is set as a fixed number for input image with arbitrary size. While, in our PGT, the group number is constant for each stage and gradually decreases from shallow stage to deep stage. The group size depends on the size of the input image. Therefore, as the image size increases, the receptive field of PGT enlarges faster than that of Swin.

**Compared with PVT.** PVT [55] proposed Spatial Reduction Attention (SRA) module to reduce the computational and

memory cost of global attention, which makes it affordable for high-resolution features. Nevertheless, the receptive fields in all stages of PVT are still global. Different from that, we propose to gradually increase the receptive fields rather than global throughout the network. Thus, our PGT does better in learning low-level features with detailed information, and high-level features with rich semantics.

### C. Feature Pyramid Transformer

To generate finer semantic image segmentation, we propose a Feature Pyramid Transformer (FPT) to aggregate the information from multiple levels of the PGT encoder, as shown in Figure 2. Inspired by the spirit of convolution-based FPN [34], FPT is expected to fuse the semantic-level representations and spatial-level information into a high-resolution and high-level semantic output.

Specifically, given the output hierarchical features  $\{F_i\}, i \in \{1, 2, \dots, L\}$  of the encoder, we first use a light-weight fusion module, containing lateral connections and a top-down pathway, to introduce strong semantics into all levels,

$$\hat{F}_i = \begin{cases} \phi(F_i) + \text{Upsample}(\hat{F}_{i+1}), & 1 \leq i < L \\ \phi(F_i), & i = L \end{cases} \quad (3)$$

where  $\phi$  is used to align the channel dimension, implemented by a linear projection layer. Upsample denotes bilinear interpolation. Note that  $\hat{F}_i$  has the same size of  $F_i$ . Then, each level feature is passed through the spatial reduction Transformer blocks [55] and progressively upsampled until it reaches 1/4 scale,

$$\tilde{F}_i = \begin{cases} \Psi(\hat{F}_i), & i = 1 \\ \left[ \text{Upsample}(\Psi(\hat{F}_i)) \right]_{\times(i-1)}, & 1 < i \leq L \end{cases} \quad (4)$$

TABLE I  
DETAILED CONFIGURATION OF OUR PGT VARIANTS.

Stage	Output Stride	Layer	PGT-T	PGT-S	PGT-B	PGT-L
1	4	Patch Transform	$P_1 = 4$ $C_1 = 64$	$P_1 = 4$ $C_1 = 96$	$P_1 = 4$ $C_1 = 96$	$P_1 = 4$ $C_1 = 128$
		PGT Block	$\begin{bmatrix} G_1 = 64 \\ H_1 = 2 \\ E_1 = 4 \end{bmatrix} \times 2$	$\begin{bmatrix} G_1 = 64 \\ H_1 = 3 \\ E_1 = 4 \end{bmatrix} \times 2$	$\begin{bmatrix} G_1 = 64 \\ H_1 = 3 \\ E_1 = 4 \end{bmatrix} \times 2$	$\begin{bmatrix} G_1 = 64 \\ H_1 = 4 \\ E_1 = 4 \end{bmatrix} \times 2$
2	8	Patch Transform	$P_2 = 2$ $C_2 = 128$	$P_2 = 2$ $C_2 = 192$	$P_2 = 2$ $C_2 = 192$	$P_2 = 2$ $C_2 = 256$
		PGT Block	$\begin{bmatrix} G_2 = 16 \\ H_2 = 4 \\ E_2 = 4 \end{bmatrix} \times 2$	$\begin{bmatrix} G_2 = 16 \\ H_2 = 6 \\ E_2 = 4 \end{bmatrix} \times 2$	$\begin{bmatrix} G_2 = 16 \\ H_2 = 6 \\ E_2 = 4 \end{bmatrix} \times 2$	$\begin{bmatrix} G_2 = 16 \\ H_2 = 8 \\ E_2 = 4 \end{bmatrix} \times 2$
3	16	Patch Transform	$P_3 = 2$ $C_3 = 256$	$P_3 = 2$ $C_3 = 384$	$P_3 = 2$ $C_3 = 384$	$P_3 = 2$ $C_3 = 512$
		PGT Block	$\begin{bmatrix} G_3 = 1 \\ H_3 = 8 \\ E_3 = 4 \end{bmatrix} \times 6$	$\begin{bmatrix} G_3 = 1 \\ H_3 = 12 \\ E_3 = 4 \end{bmatrix} \times 6$	$\begin{bmatrix} G_3 = 1 \\ H_3 = 12 \\ E_3 = 4 \end{bmatrix} \times 18$	$\begin{bmatrix} G_3 = 1 \\ H_3 = 16 \\ E_3 = 4 \end{bmatrix} \times 18$
4	32	Patch Transform	$P_4 = 2$ $C_4 = 512$	$P_4 = 2$ $C_4 = 768$	$P_4 = 2$ $C_4 = 768$	$P_4 = 2$ $C_4 = 1024$
		PGT Block	$\begin{bmatrix} G_4 = 1 \\ H_4 = 16 \\ E_4 = 4 \end{bmatrix} \times 2$	$\begin{bmatrix} G_4 = 1 \\ H_4 = 24 \\ E_4 = 4 \end{bmatrix} \times 2$	$\begin{bmatrix} G_4 = 1 \\ H_4 = 24 \\ E_4 = 4 \end{bmatrix} \times 2$	$\begin{bmatrix} G_4 = 1 \\ H_4 = 32 \\ E_4 = 4 \end{bmatrix} \times 2$

where  $\Psi$  represents Transformer blocks and Upsample is implemented by bilinear interpolation.  $[f]_{\times N}$  denotes executing function  $f$  by  $N$  times. Finally, these multi-level and high-resolution representations are fused by simple element-wise summation, and further passed through a per-pixel classification head to predict pixel-level prediction and then upsampled to the original size of input image via bilinear interpolation.

$$Y = \text{Upsample} \left( \psi \left( \sum_{i=1}^L \tilde{F}_i \right) \right), \quad (5)$$

where  $\psi$  denotes per-pixel classification head, which is implemented by a linear projection layer. Benefited by the top-down connections and multi-level aggregation, our model is able to enhance the capability of fusing multi-level semantic features with different resolutions, which is essential for dense prediction tasks.

#### IV. EXPERIMENTS

In this section, we first compare our PGT with the state-of-the-art methods on the image classification task. To further demonstrate the effectiveness of our FTN, we conduct experiments on three widely-used segmentation benchmarks, PASCAL Context [43], ADE20K [78], and COCO-Stuff [5]. Detailed ablation studies are also provided to understand the importance and impact of individual components and settings in our method.

##### A. Image Classification

In order to train our FTN on semantic image segmentation benchmarks, we first pretrained our PGT on the ImageNet

dataset [47] for obtaining pretrained weights. ImageNet dataset contains 1.3 million images with 1,000 classes. It is referred to as ImageNet-1K in this work.

**Experiment Settings.** All the variants are trained for 300 epochs on 8 V100 GPUs from scratch, with a total batch size of 512. We use AdamW [39] as the optimizer with an initial learning rate of 0.0005, cosine decay scheduler, weight decay 0.05, and 5-epoch linear warmup. For data augmentation, we follow most of the widely used settings: random horizontal flipping [48], color jitter, Mixup [72] and AutoAugment [14] and randomly cropping to  $224 \times 224$ . We also use some regularization strategies in [52], such as Label-Smoothing [49] and stochastic depth [26]. During the evaluation, the input image is resized and center-cropped to the size of  $224 \times 224$ . The top-1 accuracy is reported for comparisons.

**Results on ImageNet-1K.** Table II shows the comparison with the state-of-the-art CNN and Transformer backbones. Compare to the dominant CNNs, our PGT consistently performs better than the state-of-the-art RegNet [45] and conventional ResNet [24] with similar complexity by a large margin. For example, our PGT-S is +2% higher than RegNetY-4G and +3.5% higher than ResNet-50. The advantage of PGT is especially obvious on tiny models, with PGT-T +4.8% higher than PVT-T. For small variants, our PGT-S surpasses the nearest CvT-13 and Swin-T by +0.4% and +0.7%, respectively. Compared with larger models, our PGT-B and PGT-L exceed PVT significantly by 1~2%, and outperform the state-of-the-art Swin Transformer with similar numbers of parameters and computation budgets, *i.e.*, 83.6 vs. 83.3 and 83.4 vs. 83.0.

TABLE II  
COMPARISONS OF DIFFERENT BACKBONES FOR THE IMAGENET-1K CLASSIFICATION. OUR PGT CONSISTENTLY OUTPERFORMS OTHER MODELS WITH SIMILAR NUMBERS OF PARAMETERS AND COMPUTATIONAL BUDGETS.

Method	Input size	Params	FLOPs	Top-1 Acc. (%)
ResNet-18 [24]	224	12M	1.8G	68.5
PVT-T [55]	224	13M	1.9G	75.1
<b>PGT-T (ours)</b>	224	13M	2.1G	<b>79.9</b>
ResNet-50 [24]	224	26M	4.1G	78.5
DeiT-S [52]	224	22M	4.6G	79.8
PVT-S [55]	224	25M	3.8G	79.8
RegNetY-4G [45]	224	21M	4.0G	80.0
T2T-ViT <sub>t</sub> -14 [67]	224	22M	6.1G	80.7
TNT-S [21]	224	24M	5.2G	81.3
Swin-T [37]	224	29M	4.5G	81.3
CvT-13 [58]	224	20M	4.5G	81.6
<b>PGT-S (ours)</b>	224	28M	4.6G	<b>82.0</b>
ResNet-101 [24]	224	45M	7.9G	79.8
PVT-M [55]	224	44M	6.7G	81.2
T2T-ViT <sub>t</sub> -19 [67]	224	39M	9.8G	81.4
RegNetY-8G [45]	224	39M	8.0G	81.7
CvT-21 [58]	224	32M	7.1G	82.5
Swin-S [37]	224	50M	8.7G	83.0
<b>PGT-B (ours)</b>	224	50M	9.1G	<b>83.4</b>
PVT-L [55]	224	61M	9.8G	81.7
DeiT-B [52]	224	86M	17.5G	81.8
T2T-ViT <sub>t</sub> -24 [67]	224	64M	15.0G	82.2
TNT-B [21]	224	66M	14.1G	82.8
RegNetY-16G [45]	224	84M	16.0G	82.9
Swin-B [37]	224	88M	15.4G	83.3
<b>PGT-L (ours)</b>	224	88M	15.9G	<b>83.6</b>
ViT-B/16 [16]	384	86M	55.4G	77.9
ViT-L/16 [16]	384	307M	190.7G	76.5

## B. Semantic Image Segmentation

We evaluate the segmentation performance of our FTN on PASCAL Context [43], ADE20K [78], and COCO-Stuff [5] datasets.

**Datasets.** PASCAL Context [43] is an extension of the PASCAL VOC 2010 detection challenge. Due to the sparsity of some categories, a subset of 60 classes is more commonly used. For fair comparisons, we also use this 60 classes (59 classes and background) subset, which contains 4998 and 5105 images for training and validation, respectively. ADE20K [78] is a more challenging scene parsing dataset, which is split into 20210, 2000, and 3352 images for training, validation and testing, respectively, with 150 fine-grained object categories. COCO-Stuff-10K [5] has 9000 training images and 1000 testing images with 182 categories, which is referred as COCO-Stuff in this paper.

**Experimental Details.** We optimize our models using AdamW [39] with a batch size of 16. The total iterations are set to 80k, 160k and 100k for PASCAL Context, ADE20K, and COCO-Stuff, respectively. The initial learning rate is set to  $6e-5$  with a polynomial decay scheduler and weight decay 0.01. During training, data augmentation in all the experiments consists of three steps: (i) random horizontal flipping, (ii) random scale with factors between 0.5 and 2, (iii) random cropping 480 for PASCAL Context and 512 for ADE20K and COCO-Stuff. During inference, the multi-scale (MS) (factors vary from 0.5 to 1.75 with 0.25 as interval) mIoU is reported. For a fair comparison, we simply apply the cross-entropy loss and synchronized BN. Similar to Swin [37], we add auxiliary

loss to the output of stage 3 of PGT with the weight of 0.4. **Results on PASCAL Context.** Table III shows the results on PASCAL Context dataset. Our FTN models with PGT variants as the encoder are significantly superior to the corresponding UperNet(Swin) models with similar numbers of parameters and computation cost. For example, our FTN(PGT-S) is +4.1% higher than UperNet(Swin-T) (53.09 vs.48.99). Our FTN(PGT-L) achieves 56.05% mIoU, outperforming the UperNet(Swin-B) with 52.57% mIoU by a large margin. Surprisingly, our FTN(PGT-L) which is pretrained on ImageNet-1K even surpasses the SETR-MLA(ViT-L/16) by +0.22%, whose encoder pretrained on a larger ImageNet-21K dataset.

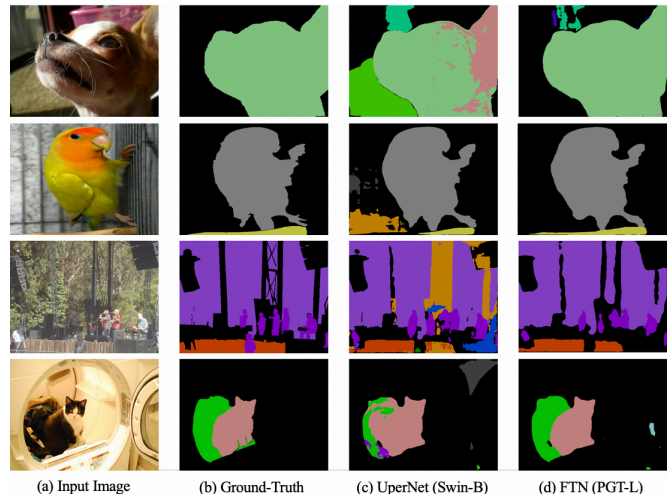


Fig. 4. Visualization comparison on PASCAL Context dataset.

**Results on ADE20K.** As shown in Table III, we compare the performance of FTN with the famous and state-of-the-art models on the more challenging ADE20K validation dataset. Compared with CNN-based models, our FTN has achieved overwhelming advantages with even a lower complexity, such as (48.68% vs. 46.35%). Compared with other Transformer segmentation models, our FTN models still outperform UperNet(Swin) under the similar computational burden. Besides, our FTN(PGT-B) achieves 50.88% mIoU, surpassing the more computationally intensive SETR-MLA(ViT-L/16).

**Results on COCO-Stuff.** The state-of-the-art results on COCO-Stuff dataset are shown in Table III. RecoNet with ResNet-101 as the backbone achieves a mIoU of 41.50%, which is the most advanced CNN model. Our FTN(PGT-T) is comparable to the most advanced CNN model (41.57 vs. 41.50) with three times reduction in the numbers of parameters. Our FTN(PGT) models are significantly superior to the promising Swin Transformers, with the advantages of about 2 ~ 3%.

**Visualization.** We illustrate the visualization results on PASCAL-Context [43], ADE20K [78] and COCO-Stuff [5] in Figure 4, Figure 5 and Figure 6, respectively. We mainly compare our FTN with UperNet [63], which performs best in previous Transformer-based segmentation methods. According to these visualizations, we can see that our FTN(PGT-L) performs better than UperNet(Swin-B) under similar computational burden in distinguishing the confusing regions with

TABLE III  
COMPARISONS WITH THE STATE-OF-THE-ART SEGMENTATION MODELS ON PASCAL CONTEXT, ADE20K AND COCO-STUFF DATASETS. ALL THE MIOU IS OBTAINED BY MULTI-SCALE INFERENCE. “ $\ddagger$ ” INDICATES PRETRAINING ON LARGER IMAGENET-21K DATASET UNDER THE INPUT SIZE OF  $384 \times 384$ . “-” MEANS NO PUBLIC RESULTS AVAILABLE.

Method	Backbone		PASCAL Context	mIoU	
	Name	Params		ADE20K	COCO-Stuff
FCN [38]	ResNet-101 [24]	45M	45.63	41.40	-
CGBNet [15]	ResNet-101 [24]	45M	53.40	44.90	37.70
PSPNet [76]	ResNet-101 [24]	45M	47.78	45.35	-
DeepLabV3+ [9]	ResNet-101 [24]	45M	48.47	46.35	-
CFNet [62]	ResNet-101 [24]	45M	52.4	-	36.6
DANet [18]	ResNet-101 [24]	45M	52.60	45.02	39.70
OCRNet [68]	ResNet-101 [24]	45M	54.80	45.28	39.50
Efficient-FCN [35]	ResNet-101 [24]	45M	53.30	45.28	-
GINet [59]	ResNet-101 [24]	45M	54.90	45.54	40.60
RecoNet [10]	ResNet-101 [24]	45M	54.80	45.54	41.50
GPSNet [19]	ResNet-101 [24]	45M	-	45.76	-
FPT [71]	ResNet-101 [24]	45M	-	45.90	-
CPNet [66]	ResNet-101 [24]	45M	53.9	46.27	-
ISNet [29]	ResNet-101 [24]	45M	-	47.55	42.08
UperNet [63]	Swin-T [37]	28M	48.99	45.81	39.13
UperNet [63]	Swin-S [37]	50M	51.66	49.47	41.58
UperNet [63]	Swin-B [37]	88M	52.57	49.72	42.20
SETR-MLA [77]	ViT-L/16 $\ddagger$ [16]	307M	55.83	50.28	-
FTN (ours)	PGT-T (ours)	13M	51.15	47.12	41.57
FTN (ours)	PGT-S (ours)	28M	53.09	48.68	43.63
FTN (ours)	PGT-B (ours)	50M	54.93	50.88	44.82
FTN (ours)	PGT-L (ours)	88M	56.05	51.36	45.89

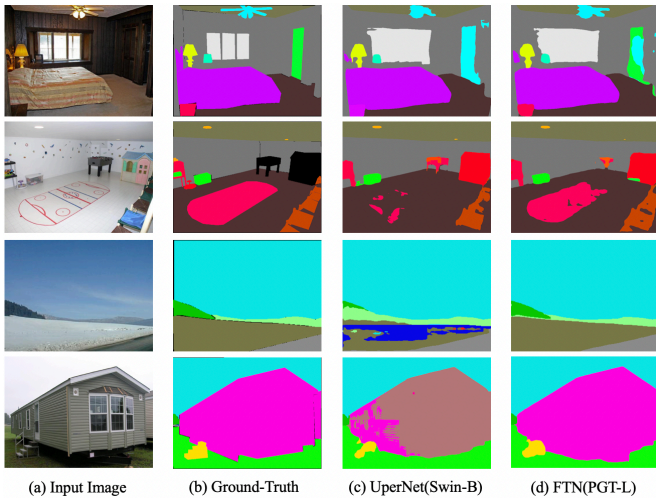


Fig. 5. Visualization comparison on ADE20K dataset.



Fig. 6. Visualization comparison on COCO-Stuff dataset.

similar colors but different categories. For example, in Line 4 of Figure 4, UperNet(Swin-B) confused the cat with its surrounding clothing, while our FTN(PGT-L) distinguish them clearly. However, UperNet(Swin-B) will confuse in some visually easy areas. For example, in the second and third row of Figure 4, the bird and its background are visually distinct, which is visually a simple scene, while UperNet(Swin-B) misjudges some part of the background surprisingly.

### C. Face Parsing

In order to evaluate the generalization of our FTN on other dense prediction tasks, we also apply our FTN(PGT-L) on the face parsing task, which aims to distinguish between different parts of the face, such as eyes, nose, and mouth.

**Dataset.** We compare our model with the state-of-the-art methods on CelebAMask-HQ dataset [32], which is a large-scale face parsing dataset with 19 categories including some additional eyeglass, earring, necklace, neck, and cloth beyond the traditional facial components. It contains 24183, 2993, and 2824 images for training, validation, and testing respectively.

TABLE IV  
COMPARISONS WITH STATE-OF-THE-ARTS ON THE CELEBAMASK-HQ DATASET (IN F1 SCORE).

Method	Face I-Mouth	Nose U-Lip	Glasses L-Lip	L-Eye Hair	R-Eye Hat	L-Brow Earring	R-Brow Necklace	L-Ear Neck	R-Ear Cloth	Mean
PSPNet [76]	94.8 89.8	90.3 87.1	75.8 88.8	79.9 90.4	80.1 58.2	77.3 65.7	78.0 19.4	75.6 82.7	73.1 64.2	76.2
MaskGAN [32]	95.5 63.4	85.6 88.9	92.9 90.1	84.3 86.6	85.2 91.3	81.4 63.2	81.2 26.1	84.9 <b>92.8</b>	83.1 68.3	80.3
EHANet [40]	96.0 93.8	93.7 88.6	90.6 90.3	86.2 93.9	86.5 85.9	83.2 67.8	83.1 30.1	86.5 88.8	84.1 83.5	84.0
Wei <i>et al.</i> [57]	96.4 90.6	91.9 87.9	89.5 91.0	87.1 91.1	85.0 83.9	80.8 65.4	82.5 17.8	84.1 88.1	83.3 80.6	82.1
EAGRNet [51]	96.2 <b>95.0</b>	94.0 88.9	92.3 91.2	88.6 94.9	88.7 87.6	85.7 68.3	85.2 27.6	88.0 89.4	85.7 85.3	85.1
AGRNet [50]	96.5 92.0	93.9 89.1	91.8 91.1	88.7 95.2	89.1 87.2	85.5 69.6	85.6 32.8	88.1 89.9	<b>88.7</b> 84.9	85.5
UperNet(Swin-B) [37]	96.5 92.1	94.0 89.4	92.1 91.2	89.7 95.5	89.9 90.1	86.2 70.5	85.9 35.4	88.3 90.3	87.9 87.1	86.2
FTN-L (ours)	<b>96.6</b> 92.4	<b>94.3</b> <b>89.9</b>	<b>93.3</b> <b>91.4</b>	<b>90.0</b> <b>96.1</b>	<b>90.3</b> <b>92.2</b>	<b>87.0</b> <b>72.0</b>	<b>86.6</b> <b>40.2</b>	<b>88.9</b> 92.2	88.5 <b>91.0</b>	<b>87.4</b>

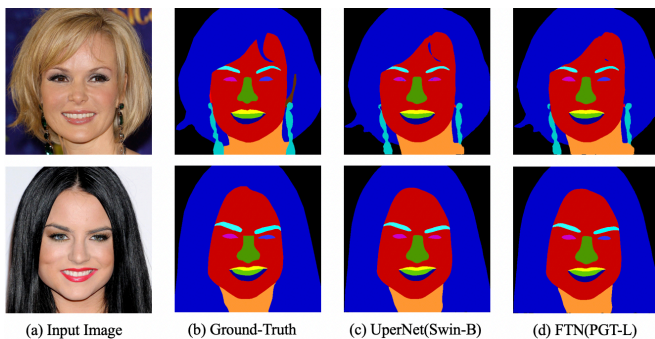


Fig. 7. Visualization comparison on CelebAMask-HQ dataset.

**Settings.** We conduct experiments on 2 V100 GPUs with a total batch size of 16. The models are trained for 160k iterations with AdamW [39] as the optimizer (weight decay=0.01). The initial learning rate is set to  $6e-5$  and decay via polynomial scheduler. Synchronized BN and cross-entropy loss are used during training.

**Results.** Table IV compares the F1 score of recent approaches. Compared with previous best CNN-based method, our FTN(PGT-L) outperforms AGRNet [50] by a large margin (87.4 vs. 85.5). Our FTN(PGT-L) also surpasses the UperNet(Swin-B) by +1.2%. Note that the backbone of both UperNet(Swin-B) and FTN(PGT-L) are pretrained on ImageNet-1k with  $224 \times 224$  input size. Figure 7 presents the visualization comparisons, which shows that the segmentation of our FTN(PGT-L) is more detailed.

#### D. Ablation Study

In this section, we first replace the encoder and decoder of our FTN with other models for comparisons to demonstrate the effectiveness of PGT and FPT, respectively. Then, we ablate the key designs of PGT, *i.e.*, group numbers, position encoding

and class token. Finally, we provide more ablation experiments for some design choices of FPT.

**Effectiveness of PGT.** Our proposed FTN is a general and flexible fully Transformer framework for image segmentation, in which the encoder can be replaced by any other Vision Transformer backbones. In order to prove the effectiveness of PGT, we compare the recent promising Transformer backbones, such as ViT [16], PVT [55] and Swin Transformer [37] with our PGT under various decoders on PASCAL Context. As shown in Table V, no matter which decoder is used, our PGT variants are about +3~6% higher than PVT variants and +2~4% higher than Swin variants on average under similar computation burdens, which demonstrates the superiority of our PGT. It is remarkable that our PGT-L even surpasses the more computationally intensive ViT-L (pretrained on ImageNet-21K) by +1~2% improvement with considerably fewer amount of pretraining data.

**Effectiveness of FPT.** Meanwhile, the decoder part of FTN is also compatible with various CNN and Transformer-based decoders. To evaluate the effectiveness of our FPT, we compare FPT with the decoders used in previous Transformer segmentation models on PASCAL Context dataset. Experiments in Table V show that no matter which backbone is applied, our FPT is consistently superior to other popular decoders, about +1% higher than Semantic FPN and about +0.5% higher than UperNet used in [37]. Compared with another query-based Transformer decoder proposed in Trans2Seg [64], our FPT also performs better by a large margin (55.24 vs. 54.13).

**Group Choices of PGT.** As mentioned in Section III-B, the receptive fields of PGT can be adjusted by the number of groups in four encoder stages. Excessive receptive fields will impose a heavy computational burden, while if the receptive field is too small, it will be insufficient for context modeling. Figure VI shows the comparison with different choices of PGT group numbers in four encoder stages. PGT<64-16-1-1> is +0.38% better than PGT<64-16-4-1> with fewer additional

TABLE V

COMBINATIONS OF DIFFERENT ENCODERS AND DECODERS ON PASCAL CONTEXT VALIDATION DATASET. ‡ REFERS TO PRETRAINING ON A LARGER IMAGENET-21K DATASET UNDER THE INPUT SIZE OF  $384 \times 384$ . FOR A FAIR COMPARISON, ALL THE SETTINGS ARE SAME AS MENTIONED IN SECTION IV-B, EXCEPT THAT THE AUXILIARY LAYERS ARE REMOVED AND THE TOTAL ITERATION IS HALVED TO 40K.

Encoder		Decoder						
		CNN				Transformer		
Model	Params	Semantic FPN [31]	SETR-PUP [77]	SETR-MLA [77]	DPT [46]	UperNet [63]	Trans2Seg [64]	FPT(ours)
PVT-T [55]	13M	43.34	41.13	43.50	43.67	43.92	43.03	44.62
PGT-T (ours)	13M	49.04	46.59	49.21	48.63	49.95	49.56	50.48
PVT-S [55]	25M	47.53	45.44	47.63	47.13	47.95	46.19	48.43
Swin-T [37]	28M	47.01	44.43	47.29	47.25	48.95	47.42	49.42
PGT-S (ours)	28M	50.37	47.94	50.91	50.67	51.58	50.83	51.93
Swin-S [37]	50M	50.03	47.10	50.77	50.51	51.76	50.17	52.43
PVT-L [55]	61M	49.70	47.20	50.27	49.52	50.53	49.72	51.08
PGT-B (ours)	50M	53.26	50.29	53.73	53.24	54.02	53.44	54.06
Swin-B [37]	88M	50.31	47.52	51.18	52.17	52.51	50.80	53.35
ViT-L/16 <sup>‡</sup> [16]	307M	52.65	52.42	52.87	52.65	52.93	52.78	53.43
PGT-L (ours)	88M	54.09	52.61	54.60	54.31	54.73	54.13	55.24

TABLE VI

DIFFERENT RECEPTIVE FIELDS OF PGT. THE A, B, C, D IN <A-B-C-D> REPRESENT THE GROUP NUMBER IN STAGE 1~4 RESPECTIVELY.

Pyramid Group Numbers	Top-1 Acc. (%)
<64-16-4-1>	77.81
<64-16-1-1>	78.19
<16-4-1-1>	<b>78.21</b>

TABLE VII

DIFFERENT POSITION ENCODING APPROACHES IN PGT.

Position Encoding	Top-1 Acc. (%)
no pos.	76.33
APE	77.49
CPE	<b>78.19</b>
APE&CPE	77.85

computation, which demonstrates that global context modeling on the 1/16 resolution features in stage3 is critical to the performance. PGT<16-4-1-1> is slightly +0.02% better than PGT<64-16-1-1>, but much more expensive for memory cost. As a result, we use PGT<64-16-1-1> in our PGT variants.

**Position Encoding of PGT.** Positional embeddings are used to introduce the awareness of spatial location for self-attention, which have been proved to be critical to Transformers [12], [16], [37], [53]. To understand the effect of position encoding methods for our PGT, we compare four different settings, namely no position encoding (no pos.), learnable absolute position encoding (APE) [16], conditional position encoding (CPE) [12] and a combination of APE and CPE (APE&CPE). As shown in Figure VII, APE achieves +1.16% higher than no pos., which shows the importance of position encoding. CPE achieves +0.7% higher than APE and +0.34% higher than APE&CPE. Furthermore, CPE is compatible with variable-length input sequences, which is an obvious limitation of absolute position encoding. Therefore, we use CPE in our PGT as an implicit position encoding scheme.

**CLS-Token of PGT.** CLS-Token plays the role of a global image representation, which is expected to contain all of

TABLE VIII

DIFFERENT CLS-TOKEN IN PGT.

CLS-Token	Top-1 Acc. (%)
stage 4	77.82
stage 1~4	77.71
avgpooling	<b>78.19</b>

TABLE IX

COMPARISONS OF DIFFERENT SETTINGS OF FPT. <A-B-C> REPRESENTS THE SETTINGS FOR THE TRANSFORMER BLOCKS WHICH ARE PERFORMED ON THE FEATURE MAPS WITH STRIDE 32("A"), 16("B") AND 8("C"), RESPECTIVELY. THE mIOU IS OBTAINED BY MULTI-SCALE INFERENCE ON COCO-STUFF VALIDATION DATASET.

Depth	Embedding dim	SR-MSA ratio	Fusion mode	mIoU (%)
<1-1-1>	256	<2-2-2>	add	42.41
<1-1-1>	512	<2-2-2>	add	<b>43.37</b>
<1-2-1>	512	<2-2-2>	add	43.11
<1-1-1>	512	<1-2-2>	add	43.26
<1-1-1>	512	<1-1-2>	add	43.33
<1-1-1>	512	<2-2-2>	concat	43.35

discriminate information for final classification. Some of Vision Transformers kept CLS-Token throughout the network [16], while some works only involved it at the last stage [55]. Considering that CLS-Token may have missed some key information, [37] directly removed the CLS-Token and applied average pooling on the last output of the backbone instead. Inspired by above all, we study the impact of four CLS-token patterns for PGT. As shown in Figure VIII, average pooling performs the best, achieving +0.37% and +0.48% higher than the CLS-token in only stage4 and all stages respectively. Thus, in PGT, we simply apply average pooling on the final output of stage 4 to generate a global token rather than CLS-Token.

**Scales of FPT.** With the limited segmentation training data, the scale of decoder is not the larger the better for segmentation [64], so that there is an important trade-off between the scale of FPT and the performance. In our FPT, the scale is mainly determined by depth, embedding dim, and the reduction ratio of SR-MSA. We compare several combinations of these hyper-parameters with PGT-S as the backbone on COCO-Stuff

validation set. All the settings are the same as Section 4.2, except the abandoned auxiliary layers.

Considering that features with stride 16 have a good trade-off in terms of containing semantic and detailed information, we try to enlarge the depth (number of blocks) for Transformer blocks with 1/16 features in FPT. As shown in Table IX, increasing the depth for 1/16 features results in a 0.26% mIoU drop (43.37 vs. 43.11), which indicates that the FPT decoder is not the deeper the better.

Embedding dim refers to the dimension of tokens in transformer blocks of FPT. Excessive small embedding dim might lead to the lack of representation ability, and a too large one may result in channel redundancy and increased computational burden. Considering the constraints of computing resources, we tried two computation-friendly choices of embedding dims ( $dim=256$  and  $512$ ). As shown in Table IX,  $dim=512$  is significantly superior to  $dim=256$  (43.37 vs. 42.41). Therefore, we set the embedding dim to 512 in our FPT.

SR-MSA is used to reduce memory and computation cost by spatially reducing the number of key and value tokens, especially for high-resolution representations. Considering that the token numbers of the low-resolution features are relatively fewer, we attempt to remove the spatial reduction for transformer blocks with 1/32 and 1/16 features. Table IX compares the different choices of reduction ratio of SR-MSA in FPT. It turns out that without using SR-MSA on low-resolution representations, the computation cost is increased, while there is no significant performance gain as expected (43.37 vs. 43.33 vs. 43.26). On the contrary, not using SR-MSA results in slight performance degradation.

**Fusion Mode of FPT.** In our FPT, the multi-level high-resolution features of each branch need to be fused to generate finer prediction. We explore two simple fusion mode, *i.e.*, element-wise summation and channel-wise concatenation. As shown in Table IX, summation performs +0.02% slightly better than concatenation, thus we fuse the multi-level representations by the simpler and more efficient element-wise summation.

## V. CONCLUSION

We have developed the Fully Transformer Networks (FTN) for semantic image segmentation. The core contributions of FTN are the proposed Pyramid Group Transformer (PGT) encoder and Feature Pyramid Transformer (FPT) decoder. The former learns hierarchical representations, which creates Pyramid Group Multi-head Self Attention to dramatically improve the efficiency and reduce the computation costs of the traditional Multi-head Self Attention. The latter fuses semantic-level and spatial-level information from multiple stages of the encoder, which can promote to the generation of finer segmentation results. Extensive experimental results on PASCAL-Context, ADE20K, and COCO-Stuff have shown that our FTN can outperform the state-of-the-art methods in semantic image segmentation, demonstrating that the Fully Transformer Networks can achieve better results than hybrid Transformer and CNN approaches.

## REFERENCES

- [1] Jimmy Lei Ba, Jamie Ryan Kiros, and Geoffrey E Hinton. Layer normalization. *arXiv preprint arXiv:1607.06450*, 2016.
- [2] Vijay Badrinarayanan, Alex Kendall, and Roberto Cipolla. Segnet: A deep convolutional encoder-decoder architecture for image segmentation. *IEEE transactions on pattern analysis and machine intelligence*, 39(12):2481–2495, 2017.
- [3] Irwan Bello, Barret Zoph, Ashish Vaswani, Jonathon Shlens, and Quoc V Le. Attention augmented convolutional networks. In *Proceedings of the IEEE/CVF International Conference on Computer Vision*, pages 3286–3295, 2019.
- [4] Shubhankar Borse, Ying Wang, Yizhe Zhang, and Fatih Porikli. Inverseform: A loss function for structured boundary-aware segmentation. In *Proceedings of the IEEE/CVF Conference on Computer Vision and Pattern Recognition*, pages 5901–5911, 2021.
- [5] Holger Caesar, Jasper Uijlings, and Vittorio Ferrari. Coco-stuff: Thing and stuff classes in context. In *Proceedings of the IEEE conference on computer vision and pattern recognition*, pages 1209–1218, 2018.
- [6] Nicolas Carion, Francisco Massa, Gabriel Synnaeve, Nicolas Usunier, Alexander Kirillov, and Sergey Zagoruyko. End-to-end object detection with transformers. In *European Conference on Computer Vision*, pages 213–229. Springer, 2020.
- [7] Liang-Chieh Chen, George Papandreou, Iasonas Kokkinos, Kevin Murphy, and Alan L Yuille. Deeplab: Semantic image segmentation with deep convolutional nets, atrous convolution, and fully connected crfs. *IEEE transactions on pattern analysis and machine intelligence*, 40(4):834–848, 2017.
- [8] Liang-Chieh Chen, George Papandreou, Florian Schroff, and Hartwig Adam. Rethinking atrous convolution for semantic image segmentation. *arXiv preprint arXiv:1706.05587*, 2017.
- [9] Liang-Chieh Chen, Yukun Zhu, George Papandreou, Florian Schroff, and Hartwig Adam. Encoder-decoder with atrous separable convolution for semantic image segmentation. In *Proceedings of the European conference on computer vision (ECCV)*, pages 801–818, 2018.
- [10] Wanli Chen, Xinge Zhu, Ruoqi Sun, Junjun He, Ruiyu Li, Xiaoyong Shen, and Bei Yu. Tensor low-rank reconstruction for semantic segmentation. In *European Conference on Computer Vision*, pages 52–69. Springer, 2020.
- [11] Bowen Cheng, Ross Girshick, Piotr Dollár, Alexander C Berg, and Alexander Kirillov. Boundary iou: Improving object-centric image segmentation evaluation. In *Proceedings of the IEEE/CVF Conference on Computer Vision and Pattern Recognition*, pages 15334–15342, 2021.
- [12] Xiangxiang Chu, Zhi Tian, Bo Zhang, Xinlong Wang, Xiaolin Wei, Huaxia Xia, and Chunhua Shen. Conditional positional encodings for vision transformers. *arXiv preprint arXiv:2102.10882*, 2021.
- [13] Marius Cordts, Mohamed Omran, Sebastian Ramos, Timo Rehfeld, Markus Enzweiler, Rodrigo Benenson, Uwe Franke, Stefan Roth, and Bernt Schiele. The cityscapes dataset for semantic urban scene understanding. In *Proceedings of the IEEE conference on computer vision and pattern recognition*, pages 3213–3223, 2016.
- [14] Ekin D Cubuk, Barret Zoph, Dandelion Mane, Vijay Vasudevan, and Quoc V Le. Autoaugment: Learning augmentation strategies from data. In *Proceedings of the IEEE/CVF Conference on Computer Vision and Pattern Recognition*, pages 113–123, 2019.
- [15] Henghui Ding, Xudong Jiang, Bing Shuai, Ai Qun Liu, and Gang Wang. Semantic segmentation with context encoding and multi-path decoding. *IEEE Transactions on Image Processing*, 29:3520–3533, 2020.
- [16] Alexey Dosovitskiy, Lucas Beyer, Alexander Kolesnikov, Dirk Weissenborn, Xiaohua Zhai, Thomas Unterthiner, Mostafa Dehghani, Matthias Minderer, Georg Heigold, Sylvain Gelly, Jakob Uszkoreit, and Neil Houlsby. An image is worth 16x16 words: Transformers for image recognition at scale. In *International Conference on Learning Representations*, 2021.
- [17] Haoqi Fan, Bo Xiong, Karttikeya Mangalam, Yanghao Li, Zhicheng Yan, Jitendra Malik, and Christoph Feichtenhofer. Multiscale vision transformers. In *Proceedings of the IEEE/CVF International Conference on Computer Vision (ICCV)*, pages 6824–6835, October 2021.
- [18] Jun Fu, Jing Liu, Haijie Tian, Yong Li, Yongjun Bao, Zhiwei Fang, and Hanqing Lu. Dual attention network for scene segmentation. In *Proceedings of the IEEE/CVF Conference on Computer Vision and Pattern Recognition*, pages 3146–3154, 2019.
- [19] Qichuan Geng, Hong Zhang, Xiaojuan Qi, Gao Huang, Ruigang Yang, and Zhong Zhou. Gated path selection network for semantic segmentation. *IEEE Transactions on Image Processing*, 30:2436–2449, 2021.
- [20] Jatin Gupta, Sumindar Kaur Saini, and Mamta Juneja. Survey of denoising and segmentation techniques for mri images of prostate for improving diagnostic tools in medical applications. *Materials Today: Proceedings*, 28:1667–1672, 2020.

- [21] Kai Han, An Xiao, Enhua Wu, Jianyuan Guo, Chunjing Xu, and Yunhe Wang. Transformer in transformer. *arXiv preprint arXiv:2103.00112*, 2021.
- [22] Matthias Harders and Gabor Szekely. Enhancing human-computer interaction in medical segmentation. *Proceedings of the IEEE*, 91(9):1430–1442, 2003.
- [23] Jun-Yan He, Shi-Hua Liang, Xiao Wu, Bo Zhao, and Lei Zhang. Mseg: Multiple granularity-based real-time semantic segmentation network. *IEEE Transactions on Image Processing*, 30:7200–7214, 2021.
- [24] Kaiming He, Xiangyu Zhang, Shaoqing Ren, and Jian Sun. Deep residual learning for image recognition. In *Proceedings of the IEEE conference on computer vision and pattern recognition*, pages 770–778, 2016.
- [25] Jeremy Howard and Sebastian Ruder. Universal language model fine-tuning for text classification. In *ACL*, 2018.
- [26] Gao Huang, Yu Sun, Zhuang Liu, Daniel Sedra, and Kilian Q Weinberger. Deep networks with stochastic depth. In *European conference on computer vision*, pages 646–661. Springer, 2016.
- [27] Zilong Huang, Chunyu Wang, Xinggang Wang, Wenyu Liu, and Jingdong Wang. Semantic image segmentation by scale-adaptive networks. *IEEE Transactions on Image Processing*, 29:2066–2077, 2020.
- [28] Zilong Huang, Xinggang Wang, Lichao Huang, Chang Huang, Yunchao Wei, and Wenyu Liu. Ccnet: Criss-cross attention for semantic segmentation. In *Proceedings of the IEEE/CVF International Conference on Computer Vision*, pages 603–612, 2019.
- [29] Zhenchao Jin, Bin Liu, Qi Chu, and Nenghai Yu. Isnet: Integrate image-level and semantic-level context for semantic segmentation. In *Proceedings of the IEEE/CVF International Conference on Computer Vision*, pages 7189–7198, 2021.
- [30] Longlong Jing, Yucheng Chen, and Yingli Tian. Coarse-to-fine semantic segmentation from image-level labels. *IEEE Transactions on Image Processing*, 29:225–236, 2020.
- [31] Alexander Kirillov, Ross Girshick, Kaiming He, and Piotr Dollár. Panoptic feature pyramid networks. In *Proceedings of the IEEE/CVF Conference on Computer Vision and Pattern Recognition*, pages 6399–6408, 2019.
- [32] Cheng-Han Lee, Ziwei Liu, Lingyun Wu, and Ping Luo. Maskgan: Towards diverse and interactive facial image manipulation. In *Proceedings of the IEEE/CVF Conference on Computer Vision and Pattern Recognition*, pages 5549–5558, 2020.
- [33] Yawei Li, Kai Zhang, Jie Zhang Cao, Radu Timofte, and Luc Van Gool. Localvit: Bringing locality to vision transformers. *arXiv preprint arXiv:2104.05707*, 2021.
- [34] Tsung-Yi Lin, Piotr Dollár, Ross Girshick, Kaiming He, Bharath Hariharan, and Serge Belongie. Feature pyramid networks for object detection. In *Proceedings of the IEEE conference on computer vision and pattern recognition*, pages 2117–2125, 2017.
- [35] Jianbo Liu, Junjun He, Jiawei Zhang, Jimmy S Ren, and Hongsheng Li. Efficientfcn: Holistically-guided decoding for semantic segmentation. In *European Conference on Computer Vision*, pages 1–17. Springer, 2020.
- [36] Mingyuan Liu, Dan Schonfeld, and Wei Tang. Exploit visual dependency relations for semantic segmentation. In *Proceedings of the IEEE/CVF Conference on Computer Vision and Pattern Recognition*, pages 9726–9735, 2021.
- [37] Ze Liu, Yutong Lin, Yue Cao, Han Hu, Yixuan Wei, Zheng Zhang, Stephen Lin, and Baining Guo. Swin transformer: Hierarchical vision transformer using shifted windows. In *Proceedings of the IEEE/CVF International Conference on Computer Vision (ICCV)*, pages 10012–10022, October 2021.
- [38] Jonathan Long, Evan Shelhamer, and Trevor Darrell. Fully convolutional networks for semantic segmentation. In *Proceedings of the IEEE conference on computer vision and pattern recognition*, pages 3431–3440, 2015.
- [39] Ilya Loshchilov and Frank Hutter. Decoupled weight decay regularization. In *ICLR*, 2019.
- [40] Ling Luo, Dingyu Xue, and Xinglong Feng. Ehanet: An effective hierarchical aggregation network for face parsing. *Applied Sciences*, 10(9):3135, 2020.
- [41] Wenjie Luo, Yujia Li, Raquel Urtasun, and Richard S. Zemel. Understanding the effective receptive field in deep convolutional neural networks. In *NIPS*, 2016.
- [42] Bryan McCann, James Bradbury, Caiming Xiong, and Richard Socher. Learned in translation: Contextualized word vectors. In *NIPS*, 2017.
- [43] Roozbeh Mottaghi, Xianjie Chen, Xiaobai Liu, Nam-Gyu Cho, Seong-Whan Lee, Sanja Fidler, Raquel Urtasun, and Alan Yuille. The role of context for object detection and semantic segmentation in the wild. In *Proceedings of the IEEE Conference on Computer Vision and Pattern Recognition*, pages 891–898, 2014.
- [44] Hyeonwoo Noh, Seunghoon Hong, and Bohyung Han. Learning deep convolution network for semantic segmentation. In *Proceedings of the IEEE international conference on computer vision*, pages 1520–1528, 2015.
- [45] Ilija Radosavovic, Raj Prateek Kosaraju, Ross Girshick, Kaiming He, and Piotr Dollár. Designing network design spaces. In *Proceedings of the IEEE/CVF Conference on Computer Vision and Pattern Recognition*, pages 10428–10436, 2020.
- [46] René Ranftl, Alexey Bochkovskiy, and Vladlen Koltun. Vision transformers for dense prediction. In *Proceedings of the IEEE/CVF International Conference on Computer Vision (ICCV)*, pages 12179–12188, October 2021.
- [47] Olga Russakovsky, Jia Deng, Hao Su, Jonathan Krause, Sanjeev Satheesh, Sean Ma, Zhiheng Huang, Andrej Karpathy, Aditya Khosla, Michael Bernstein, et al. Imagenet large scale visual recognition challenge. *International journal of computer vision*, 115(3):211–252, 2015.
- [48] Christian Szegedy, Wei Liu, Yangqing Jia, Pierre Sermanet, Scott Reed, Dragomir Anguelov, Dumitru Erhan, Vincent Vanhoucke, and Andrew Rabinovich. Going deeper with convolutions. In *Proceedings of the IEEE conference on computer vision and pattern recognition*, pages 1–9, 2015.
- [49] Christian Szegedy, Vincent Vanhoucke, Sergey Ioffe, Jon Shlens, and Zbigniew Wojna. Rethinking the inception architecture for computer vision. In *Proceedings of the IEEE conference on computer vision and pattern recognition*, pages 2818–2826, 2016.
- [50] Gusi Te, Wei Hu, Yinglu Liu, Hailin Shi, and Tao Mei. Agrnet: Adaptive graph representation learning and reasoning for face parsing. *IEEE Transactions on Image Processing*, 2021.
- [51] Gusi Te, Yinglu Liu, Wei Hu, Hailin Shi, and Tao Mei. Edge-aware graph representation learning and reasoning for face parsing. In *European Conference on Computer Vision*, pages 258–274. Springer, 2020.
- [52] Hugo Touvron, Matthieu Cord, Matthijs Douze, Francisco Massa, Alexandre Sablayrolles, and Hervé Jégou. Training data-efficient image transformers & distillation through attention. In *International Conference on Machine Learning*, pages 10347–10357. PMLR, 2021.
- [53] Ashish Vaswani, Noam Shazeer, Niki Parmar, Jakob Uszkoreit, Llion Jones, Aidan N Gomez, Łukasz Kaiser, and Illia Polosukhin. Attention is all you need. In *Advances in neural information processing systems*, pages 5998–6008, 2017.
- [54] Qiurui Wang, Chun Yuan, and Yan Liu. Learning deep conditional neural network for image segmentation. *IEEE Transactions on Multimedia*, 21(7):1839–1852, 2019.
- [55] Wenhai Wang, Enze Xie, Xiang Li, Deng-Ping Fan, Kaitao Song, Ding Liang, Tong Lu, Ping Luo, and Ling Shao. Pyramid vision transformer: A versatile backbone for dense prediction without convolutions. In *Proceedings of the IEEE/CVF International Conference on Computer Vision (ICCV)*, pages 568–578, October 2021.
- [56] Xiaolong Wang, Ross Girshick, Abhinav Gupta, and Kaiming He. Non-local neural networks. In *Proceedings of the IEEE conference on computer vision and pattern recognition*, pages 7794–7803, 2018.
- [57] Zhen Wei, Si Liu, Yao Sun, and Hefei Ling. Accurate facial image parsing at real-time speed. *IEEE Transactions on Image Processing*, 28(9):4659–4670, 2019.
- [58] Haiping Wu, Bin Xiao, Noel Codella, Mengchen Liu, Xiyang Dai, Lu Yuan, and Lei Zhang. Cvt: Introducing convolutions to vision transformers. In *Proceedings of the IEEE/CVF International Conference on Computer Vision (ICCV)*, pages 22–31, October 2021.
- [59] Tianyi Wu, Yu Lu, Yu Zhu, Chuang Zhang, Ming Wu, Zhanyu Ma, and Guodong Guo. Ginet: Graph interaction network for scene parsing. In *European Conference on Computer Vision*, pages 34–51. Springer, 2020.
- [60] Tianyi Wu, Sheng Tang, Rui Zhang, Juan Cao, and Jintao Li. Tree-structured kronecker convolutional network for semantic segmentation. In *2019 IEEE International Conference on Multimedia and Expo (ICME)*, pages 940–945. IEEE, 2019.
- [61] Tianyi Wu, Sheng Tang, Rui Zhang, Juan Cao, and Yongdong Zhang. Cgnet: A light-weight context guided network for semantic segmentation. *IEEE Transactions on Image Processing*, 30:1169–1179, 2020.
- [62] Tianyi Wu, Sheng Tang, Rui Zhang, and Guodong Guo. Consensus feature network for scene parsing. *IEEE Transactions on Multimedia*, 2021.
- [63] Tete Xiao, Yingcheng Liu, Bolei Zhou, Yuning Jiang, and Jian Sun. Unified perceptual parsing for scene understanding. In *Proceedings of the European Conference on Computer Vision (ECCV)*, pages 418–434, 2018.
- [64] Enze Xie, Wenjia Wang, Wenhai Wang, Peize Sun, Hang Xu, Ding Liang, and Ping Luo. Segmenting transparent objects in the wild with transformer. In Zhi-Hua Zhou, editor, *Proceedings of the Thirtieth International Joint Conference on Artificial Intelligence, IJCAI-21*, pages

- 1194–1200. International Joint Conferences on Artificial Intelligence Organization, 8 2021. Main Track.
- [65] Saining Xie, Ross Girshick, Piotr Dollár, Zhuowen Tu, and Kaiming He. Aggregated residual transformations for deep neural networks. In *Proceedings of the IEEE conference on computer vision and pattern recognition*, pages 1492–1500, 2017.
- [66] Changqian Yu, Jingbo Wang, Changxin Gao, Gang Yu, Chunhua Shen, and Nong Sang. Context prior for scene segmentation. In *Proceedings of the IEEE/CVF Conference on Computer Vision and Pattern Recognition*, pages 12416–12425, 2020.
- [67] Li Yuan, Yunpeng Chen, Tao Wang, Weihao Yu, Yujun Shi, Zi-Hang Jiang, Francis E.H. Tay, Jiashi Feng, and Shuicheng Yan. Tokens-to-token vit: Training vision transformers from scratch on imagenet. In *Proceedings of the IEEE/CVF International Conference on Computer Vision (ICCV)*, pages 558–567, October 2021.
- [68] Yuhui Yuan, Xilin Chen, and Jingdong Wang. Object-contextual representations for semantic segmentation. In *ECCV*, 2020.
- [69] Yuhui Yuan, Jingyi Xie, Xilin Chen, and Jingdong Wang. Segfix: Model-agnostic boundary refinement for segmentation. In *European Conference on Computer Vision*, pages 489–506. Springer, 2020.
- [70] Matthew D Zeiler and Rob Fergus. Visualizing and understanding convolutional networks. In *European conference on computer vision*, pages 818–833. Springer, 2014.
- [71] Dong Zhang, Hanwang Zhang, Jinhui Tang, Meng Wang, Xiansheng Hua, and Qianru Sun. Feature pyramid transformer. In *European Conference on Computer Vision*, pages 323–339. Springer, 2020.
- [72] Hongyi Zhang, Moustapha Cisse, Yann N. Dauphin, and David Lopez-Paz. mixup: Beyond empirical risk minimization. In *International Conference on Learning Representations*, 2018.
- [73] Hang Zhang, Kristin Dana, Jianping Shi, Zhongyue Zhang, Xiaogang Wang, Amrbrish Tyagi, and Amit Agrawal. Context encoding for semantic segmentation. In *Proceedings of the IEEE conference on Computer Vision and Pattern Recognition*, pages 7151–7160, 2018.
- [74] Pengchuan Zhang, Xiyang Dai, Jianwei Yang, Bin Xiao, Lu Yuan, Lei Zhang, and Jianfeng Gao. Multi-scale vision longformer: A new vision transformer for high-resolution image encoding. In *Proceedings of the IEEE/CVF International Conference on Computer Vision (ICCV)*, pages 2998–3008, October 2021.
- [75] Yang Zhang, Moyun Liu, Jingwu He, Fei Pan, and Yanwen Guo. Affinity fusion graph-based framework for natural image segmentation. *IEEE Transactions on Multimedia*, pages 1–1, 2021.
- [76] Hengshuang Zhao, Jianping Shi, Xiaojuan Qi, Xiaogang Wang, and Jiaya Jia. Pyramid scene parsing network. In *Proceedings of the IEEE conference on computer vision and pattern recognition*, pages 2881–2890, 2017.
- [77] Sixiao Zheng, Jiachen Lu, Hengshuang Zhao, Xiatian Zhu, Zekun Luo, Yabiao Wang, Yanwei Fu, Jianfeng Feng, Tao Xiang, Philip HS Torr, et al. Rethinking semantic segmentation from a sequence-to-sequence perspective with transformers. In *Proceedings of the IEEE/CVF Conference on Computer Vision and Pattern Recognition*, pages 6881–6890, 2021.
- [78] Bolei Zhou, Hang Zhao, Xavier Puig, Tete Xiao, Sanja Fidler, Adela Barriuso, and Antonio Torralba. Semantic understanding of scenes through the ade20k dataset. *International Journal of Computer Vision*, 127(3):302–321, 2019.
- [79] Zhen Zhu, Mengde Xu, Song Bai, Tengting Huang, and Xiang Bai. Asymmetric non-local neural networks for semantic segmentation. In *Proceedings of the IEEE/CVF International Conference on Computer Vision*, pages 593–602, 2019.